Silicon (2022) 14:12781–12788
https://doi.org/10.1007/s12633-022-01977-0

ORIGINAL PAPER

# Broadband Low Reflection Surfaces with Silicon Nanopillar Hexagonal Arrays for Energy Harvesting in Photovoltaics

**Turgut Tut**[1]

Received: 23 February 2022 / Accepted: 11 June 2022 / Published online: 25 June 2022


## Abstract

In this study, optimization of the silicon nanopillar arrays and thin films coated on silicon substrate has been investigated in order to minimize the optical reflection loss from the silicon substrate surface. Nanopillars's filling ratio, pillar height, pillars diameter, sidewall incline angle, and step coverage with dielectric thin film thickness are systematically optimized together for the first time with these type of nanostructures. Full-field Finite Difference Time Domain method is used to simulate electro-magnetic fields and calculate the reflection from the modified nanostructured substrate surfaces in 400-1100 nm spectral range. Optimization recipe is clearly presented and this is not only useful for hexagonal arrays but also for regular arrays of nanopillars in general. We also further decrease the reflection by using step coverage concept which is the result of nonconformal coating on steps and trenches of thin films. We obtained approximately 2% of weighted average reflection in the 400-1100 nm range for perpendicular incident solar radiation which is one of the best results reported for this type of nanostructured surfaces in the literature.

**Keywords** Nanopillars · Hexagonal array · Nonconformal deposition · Low reflection

## 1 Introduction

In general, crystalline silicon based photonic devices such as photodiodes, solar cells, phototransistors need low surface reflectance over a wide spectrum of light in order to have high external quantum efficiency and energy harvesting through outer circuits. This is the case for any type of photonic devices that operate via the optical absorption in its active layer. One of the conventional method to reduce optical surface reflection is to use single layer dielectric at specific wavelength but this does not reduce reflectivity for broadband spectrum. $SiO_2$, $SiN_x$, $TiO_2$, $Al_2O_3$ dielectric materials are the most popular thin film materials for antireflection coatings. Double dielectric layers usage for this purpose results in two reflection minimums in the reflection spectrum. In order to achieve a broadband low reflection, multi layer band pass filter could be used but this requires many thin film layers and this increases the production costs. Surface modification is needed in order to obtain broadband low reflection from the optoelectronic substrate surfaces. This modification can be achieved by using micro [1] or nano-size structures [2–12] over the device surfaces. In order to build such small features, researchers use mainly wet etching [13] and dry etching methods. For example, industrial pyramidal surface texturing for crystalline silicon uses anisotropic wet-etching method. In other methods, dry etching can be used with ionized gases in the plasma vacuum chambers. For some studies both etching methods are used in combination.

Some researchers add on some degree of randomness [6, 14] in the periodic structures to decrease the reflection loss further. However, for large area applications this can have some advantages as well as disadvantages as to have some standard way of production is not possible for these random structures.

Sizes of these structures show differences in these applications. Some applications use micro-meter size pillars [1] and some applications use nano-meter size pillars [15–17].

To summarize, recently several types of surface nanostructures have been investigated. Moth-eye nano-pyramidal pillars which use graded index refractive index to reduce reflection. Nanowires and nanocylinders that use Mie resonances (scattering) which result in overall decrease in

✉ Turgut Tut
turgut.tut@agu.edu.tr

[1] Department of Nanotechnology Engineering, Abdullah Gul University, Kayseri, Turkey

reflection. Metallic nanoparticles used their plasmonic effect to direct electromagnetic energy through the substrate effectively and decrease the reflection from the surface. These are basically light trapping mechanisms which efficiently diffract the incident light into the semiconductor [15–28].

However, in order to decrease the reflection even further, anti-reflection coating and light trapping should be used efficiently [18, 20, 29]. Some groups use hexagoal arrays for this objective [18–20]. Some studies suggest the importance of photonic crystals in these structures [30, 31]. In our work, we optimized the hexagonal nano-cone arrays in terms of photonic structure array's filling ratio, pillar height, pillar diameter, pillar angle, antireflection coating thickness, and nonconformal coating of dielectric at the same time. As a result, we get one of the lowest weighted average reflection from such structures in the literature using only one layer of dielectric thin film.

Optimization studies of the nanostructured surfaces in optoelectronic devices are still popular since the energy sector is very crucial for the economy of the countries. Even 1% increase in energy efficiency in solar cells means millions of dollars of saving in countries economies. In order to obtain high efficiency in solar cells, low optical reflection from the surfaces irrespective of incident angles in wide wavelength spectrum is needed. In this study, we choose the vertical radiation incidence, however, other studies show that this type of optimization recipes work for a range of incident angles up to 60 degrees [18, 20, 29].

In our study, we optimized nanopillars filling ratio, pillar height, pillar diameter, pillar wall angle with the vertical, with respect to the weighted average reflection to get overall efficiency improvement for the optoelectronic devices. We focused on nanopillar arrays of hexagonal type. We made use of scattering of the incident light with the truncated cone structures and nonconformal coating and the absorption of light in the photonic crystal of the periodic nanopillar array structure.

## 2 Methods and Simulation Results

In this article, we present the optimization of the nanopillar hexagonal arrays in order to achieve broadband low reflection surfaces. When compared to a bare planar crystalline silicon wafer surface, the modified surface has significant reduction in optical reflection in 400-1100 nm spectral range.

We use Full-field Finite Difference Time Domain (FDTD) method to simulate photonic nanostructures. We place power monitors just below the nanopillars to calculate the transmission to the bulk substrate. We also place a power monitor above the structure and light source to simulate the EM fields and calculate the reflected power. We used periodic boundary conditions in the simulations. Mesh size is 0.25 nm. **a** denotes the pitch size (the distance from center to center of the nanopillars). Since the structure is hexagonal, we have to define the unit cell containing two primitive cells as shown in the Fig. 1a in the simulations and it is easier to generate the structure from this unit cell. We also calculate the light absorbed in the nanostructure. The optical constants of crystalline Si structure and dielectric thin films are taken from [32]. We first optimize the filling ratio (**d/a**) of the nanopillar arays, then height to minimize the reflection. We also varied the pillar wall angle to create truncated cones to search the effect of cone structure architechture to the reflection properties. We used dielectric anti-reflection coatings with $SiO_2$ thin film to decrease the reflection further. These nanocone truncated pillar structures can be fabricated using e-beam lithography and dry etching techniques. Due to the nature of etching processes, the vertical pillars can be obtained under special physical and chemical conditions [33, 34]. It is important to have optimized pillars inclination to get minimum reflection from such structures since as the pillar angle gets lower, the reflection starts to increase. For large area applications, nano-imprint lithography can be used with a previously prepared template using nano-fabrication methods.

Solar irradiance differs with wavelength, we can use the total reflection of light from the surface weighted with solar irradiance. This way, the low reflection loss performance can be quantified better. ASTM Air Mass 1.5 direct solar irradiance is used for the calculation. In this formulation, irradiance is multiplied with the wavelength and the integral is taken over wavelength. The numerator is composed of irradiance multiplied with wavelength and reflection. For a random polarization condition, both TE and TM polarizations are calculated and the average is taken to get more realistic result. We used the formula given below in calculating the weighted average reflection in 400-1100 nm wavelength range.

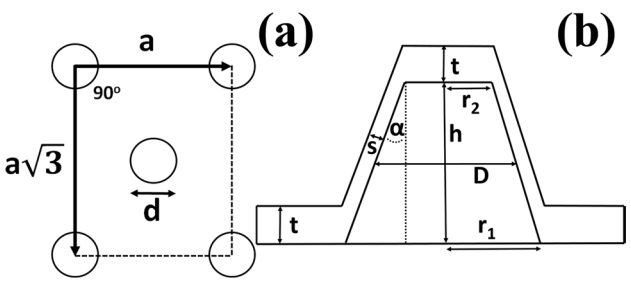


**Fig. 1** (**a**) Unit cell of hexagonal pillar array, (**b**) Cross section of truncated pillar and nonconformal coating of $SiO_2$

$$Weighted\ Average\ Reflection = \frac{\int_{400}^{1100} \frac{R_{TE}(\lambda)+R_{TM}(\lambda)}{2} I(\lambda)\lambda d\lambda}{\int_{400}^{1100} I(\lambda)\lambda d\lambda} \quad (1)$$

Figure 1a shows the unit cell of the hexagonal periodic array structure with the vertical and horizontal periodicity. Figure 1b depicts the cross section of a truncated cone nanopillar architecture. **D** is the average diameter of the cone. **r1** and **r2** are the bottom and top radii of the pillars. **h** is the height of the pillar. **α** is the angle with which the pillar wall makes with the vertical. **s** is the dialectric thickness on the sidewall of the silicon pillar and **t** is the thickness of the dialectric film coated on the top of the silicon pillar. We used this structure parameters in the photonic simulations.

As a first step, we fixed the diameter of the pillars as **d** = 230 nm, filling ratio is defined as **d/a**, pillar height is taken as **h** = 200 nm and varied the ratio of pillar diameter to period of pillar array a which is **d/a** and varied that from 0.2 to 1.0. Minimum weighted average reflection is obtained as 9.2% at **d/a** = 0.6 as depicted in Fig. 2. The reflection is low for filling ratio between 0.5 and 0.7 but the local minimum is obtained at 0.6. We used the starting dimensions from the papers from Table 1 and also we are restricted that these structures has to be micro-nano fabrication compliant. If the structure is taller than 0.5 microns then the photolithographic processes to fabricate the photovoltaic devices will face problems because the micro-nano fabrication processes need flat substrate surfaces as much as possible.

For applications that need thin film silicon layers, nanometer size structures have to be used in order to achieve low reflection in broadband. If the pillars are tall then this can lead to quantum efficiency loss due to charge recombination in the pillar structure itself and the generated electron hole pairs cannot be extracted from the devices for energy harvesting. Thus, the height of the pillars should be optimized to get low reflectivity with high quantum efficiency. When the height of the pillars are too short then the coupling of the incident light into the silicon substrate is low.

As a second step, we fixed the filling ratio as 0.6 and pillar diameter as 200 nm, we varied the pillar height from 0 to 500 nm which is depicted in Fig. 3. The minimum weighted averaged reflection is obtained for 140 nm diameter as approximately 5.25% over 400-1100 nm range. Since we are dealing with the thin film device applications, we take the height range 0-500 nm, since taller or shorter height nanopillar arrays have high reflectivity in the interested spectral region. As depicted in Fig. 3, we varied the height of the pillars and we found that 140 nm is the optimum height especially for low reflection in 400-1100 nm range. For large pillar heights, the reflectivity increases especially for UV region in the spectrum. For shorter pillars, the reflection increases especially for wavelengths larger than 600 nm. We try to keep the range as large as possible but we set the lower and upper limits as 0 and 500 nm respectively for micro-nano fabrication considerations.

As a third step, the height of the pillar is taken as 140 nm, the diameter is varied from 50 to 500 nm and the minimum reflection is obtained at 200 nm as 4.54%. Figure 4 depicts the weighted average reflection versus nanopillar diameter. We try to keep the range as large as possible in case there is another local minimum in the weighted averaged reflection. Again we are restricted with the same fabrication considerations.As the pillar diameter increases above 200 nm, the incident light reflects from the flat surface of the pillars. As the pillar diameter decreases below 200 nm, the incident light reflects from the Si wafer surface. Therefore, in both cases, the reflection increases only about 200 nm diameter,

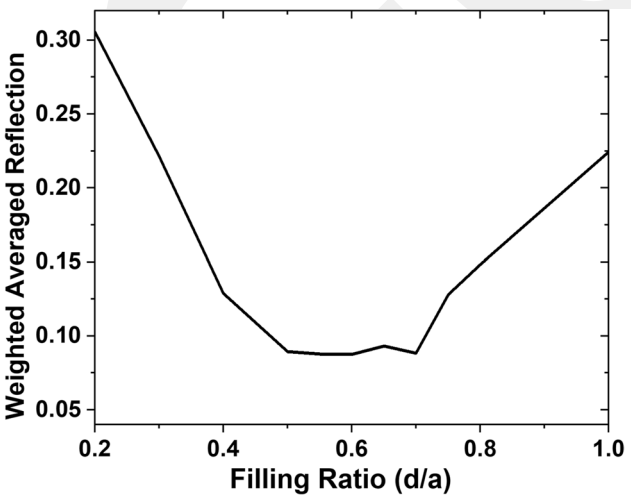


**Fig. 2** Weighted average reflection versus filling ratio of the hexagonal array

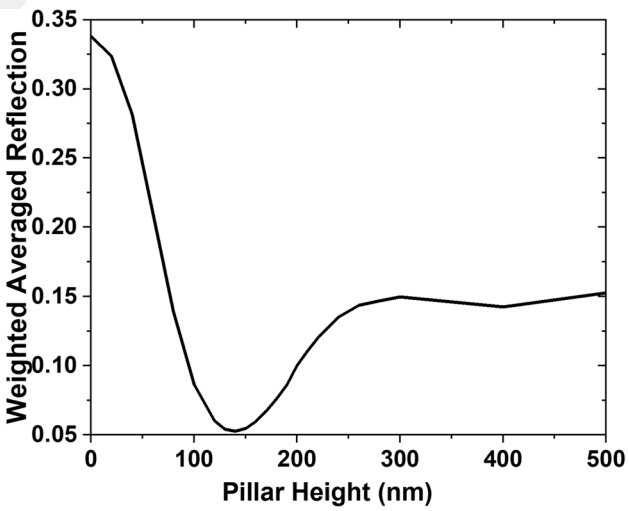


**Fig. 3** Height optimization of the pillars

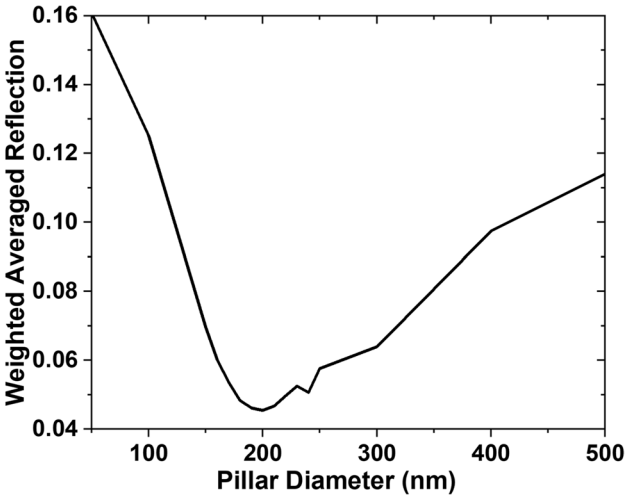


**Fig. 4** Weighted average reflection versus pillar diameter

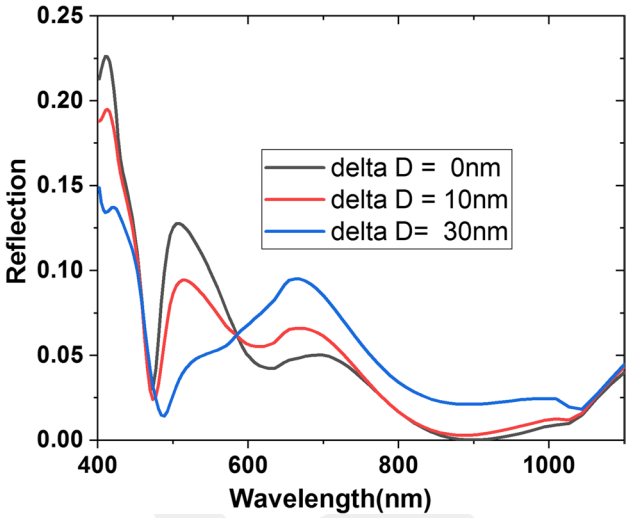


**Fig. 6** Reflection spectra with solar irradiance on earth surface versus pillar angle

the incident light couples better to the structure and reflection gets lower.

As a fourth step, the slope of the pillars is varied. **Delta D** means the difference between the bottom diameter and top diameter of the pillars. We call these pillars as truncated cone pillars. The minimum reflection occurs at 10 nm diameter difference and the reflection is about 4.48%. This slope angle is approximately 4.1 degrees. In Fig. 5, the local minimum can be clearly seen. In Fig. 6, the reflection spectrum is shown for diameter differences of 0, 10 nm, and 30 nm. As the angle is increased further, the reflection decreased below 650 nm but it increases above 650-1100 nm range. For specific range of wavelengths, this property can be useful. It is important to fabricate pillars close to vertical.

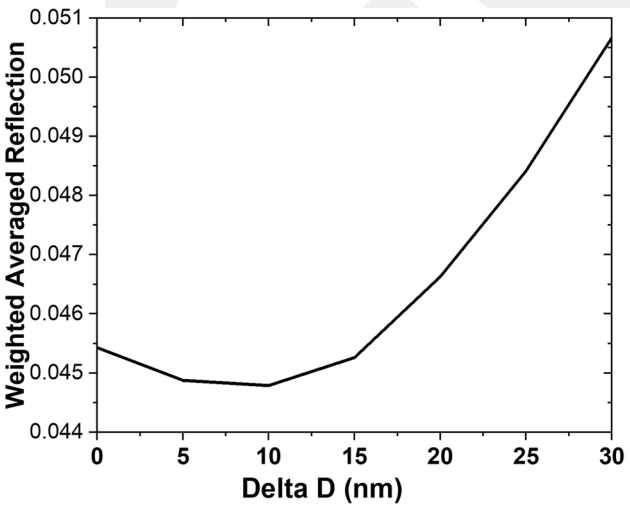


**Fig. 5** Weighted average reflection versus pillar slope

Truncated nanopillars apex angle can be controlled with optimizing the dry etching conditions, e.g., chamber pressure, gas flow rates ratio, RF power, coil power.

We further examine the anti-reflection dielectric film $SiO_2$ thin film coating and it is first assumed to be conformal coating. In Fig. 4, from bare Si pillars to 50 nm thin film $SiO_2$ added at top of the nanopillar structures. As can be noticed, the reflection is minimum and small in about 15 nm range around the minimum [35]. At other spectral wavelength range 400-1100 nm, the reflection is even larger than we obtained when only nano pillar arrays are used. Therefore, instead of using the concept of antireflection minimization at one point, the analysis of a range of thin film thickness is needed using FDTD simulations optimized according to weighted averaged reclection over 400-1100 nm spectral range. The reflection of 4.21% is obtained for 15 nm $SiO_2$ thin film which is shown in Fig. 7. We set the upper limit at 50 nm for dielectric thin film since for conformal coatings we expect only one local minimum from the earlier studies from Table 1.

In order to achieve even lower reflection, we used the property of nonconformal coating of dielectric materials on step structures. Since the nano-pillar structures create a step, the coating thickness on the sidewall is generally thinner than the coating thickness on top of the pillars. Therefore, we fixed the optimized conformal thickness of the $SiO_2$ dielectrics on the sidewall but varied the thickness on top. When the dielectric thickness, on top of the pillar is increased, the weighted average reflection is reduced considerably. In Fig. 8a), when $SiO_2$ is coated conformally with 15 nm thckness, the reflection gets lower over the visible range with respect to the no $SiO_2$ coating case. But when the coating is nonconformal with **s/t** = 0.2, then the reflection

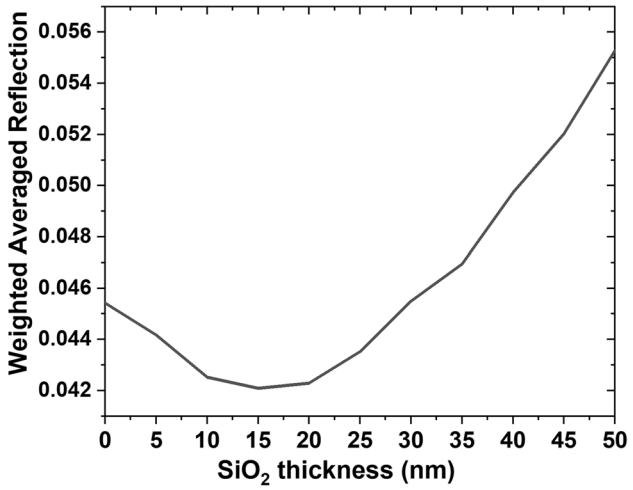


**Fig. 7** Anti-reflection dielectric $SiO_2$ thin film coating on the nanopillar array

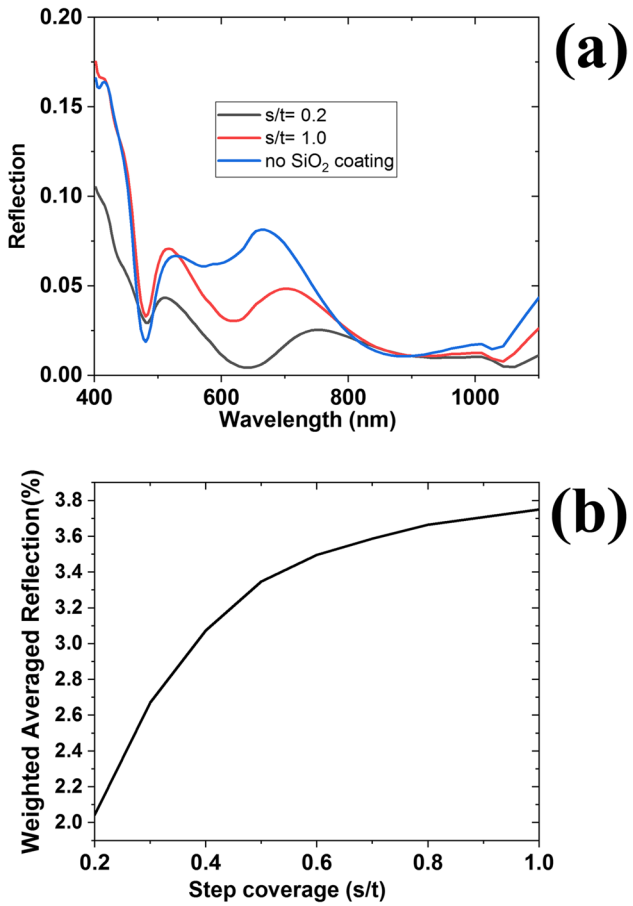


**Fig. 8** Reflection versus wavelength with **s/t** $SiO_2$ thin film ratio

gets reduced almost everywhere over the 400-1100 nm range. The reflection loss is 2.045% for **s/t** = 0.2 nonconformal coating. This result is the lowest average reflection

**Table 1** Comparison of recent results for the average reflections from regular square and hexagonal nanopillar arrays

| Author | Year | R (Average) |
|---|---|---|
| J. Li et al. [38] | 2009 | >10% |
| C. Lin et al. [39] | 2011 | 4.64% |
| J. Proust et al. [40] | 2016 | 4% |
| J. Kim et al. [41] | 2021 | 7.1% |
| A. V. Guardado et al. [36] | 2018 | 3% |
| W. Yan et al. [37] | 2016 | 2.1% |

from such nanostructured surfaces with one dielectric thin film coating. Several recent results and their comparison is given in Table 1. Especially, the works reported in references [36, 37] have the hexagonal nanostructures. The Guardado et al. work reports non-conformal $SiO_2$ layer coated over the pillar array structure simulation in 400-1100 nm range and achieves 3% wavelength averaged reflection. Their optimized silicon pillar array structure has the parameters of **a** = 500 nm, **d** = 300 nm, **h** = 140 nm. The W. Yan et al. work reports conformal $TiO_2$ coating over the silicon pillar arrays in 460-1040 nm range and achieves 2.1% wavelength averaged reflection. Their optimized pillar array structure has the parameters of **d**(bottom) = 240 nm, **d**(top) = 220 nm, and **a** = 460 nm, **h** = 200 nm. Their result however should be larger when the average is taken over 400-1100 nm since below 450 nm and above 1000 nm the reflection is relatively larger.

It is also notable that the reflection is relatively high for the UV spectral region below 450 nm wavelength Fig. 8a. This is due to the fact that at small wavelengths, the light rays start to ignore the nanopillar array structure and get reflected from the bare silicon substrate surface. Therefore, reflection loss is high for UV region. The plasma enhanced vapor deposition systems, low pressure vapor deposition, e-beam evaporation, and sputtering systems are known to have nonconformal coating property. We will pursue this issue in our next study experimentally by optimizing the deposition conditions, e.g. chamber pressure, deposition gas flow rates, substrate temperature, RF power. It can also be seen in Fig. 8b that the reflectivity is reduced even further for **s/t** ratio lower than 0.2. However, this may not be achievable experimentally. We will investigate this **s/t** ratio lower limit experimentally in our future study.

We also realized that in order to increase the efficiency of photonic devies, we have to increase the optical power absorbed in the bulk of the active silicon layer. The absorbed light in the nanostructures could be lost due to recombination and cannot contribute to the photocurrent with large percentage. Therefore, we have to maximize the absorption not in the nanostructures but in the bulk silicon active device region. For the deep UV region it is

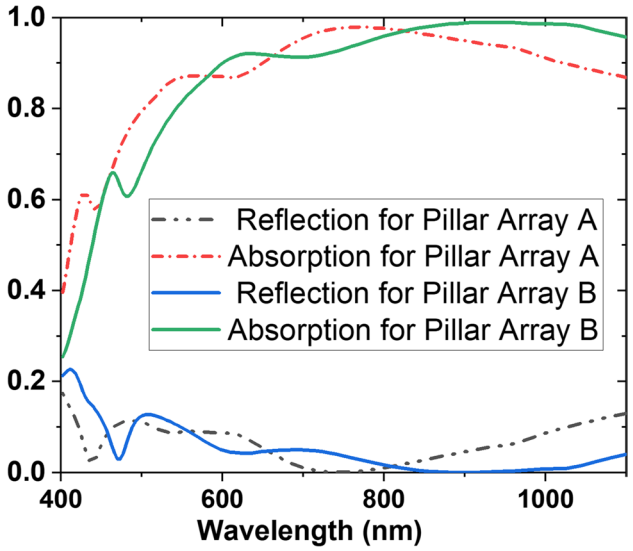


**Fig. 9** Comparison of optimized silicon nanopillar arrays. Pillar array A is optimized according to high optical absorption in the bulk. Pillar array B is optimized according to low optical reflection

a hard job to realize that due to the high absorption (Light absorption coefficient for silicon increases about 6 orders from 1100 nm to 400 nm ). However in 400-1100 nm range, it is possile to optimize the nano-size pillar array structure in order to achieve low reflection. In this paper, we emphasize the nanostructure surfaces with low reflection. However, it is a good idea to compare the structures which are optimized according to low optical reflection and high optical absorption in the active region. When the structure is optimized in terms of high optical absorption in the active region, the optimized structure parameters are found as $\mathbf{d/a} = 0.55$, $\mathbf{d} = 170$ nm, $\mathbf{h} = 120$ nm. When the structure is optimized in terms of low reflection, the optimized structure parameters are found as $\mathbf{d/a} = 0.6$, $\mathbf{d} = 200$ nm, $\mathbf{h} = 140$ nm. Figure 9 shows the reflection and absorption spectrum of both structures. Pillar array **A** which is optimized according to absorption, has higher optical reflection above 800 nm and higher optical absorption below 800 nm compared to pillar array **B**. Weighted averaged reflection is found as 6.072% for pillar A and 4.54% for pillar array **B**. Weighted averaged absorption is found as 89.05% for pillar array **A** and 88.64% for pillar array **B**. As expected, pillar array **A** has slightly larger absorption but the actual photocurrent comparison should be made with photovoltaic devices in order to see the effect of recombination of charge carriers in the nanopillar area and the bulk region. We will investigate this issue experimentally in another study.

## 3 Conclusions

The reflection properties of the nanostructured silicon surfaces have been investigated and understood physically through weighted average reflection as a function of wavelength in 400-1100 nm range. We see that using truncated nanocones has potential to reduce further the total weighted reflection loss from the surface of the photonic devices for specific wavelength range. For broadband low reflection truncated cone shape nanopillars with nonconformal coated dielectric films should be used in hexagonal pillar arrays. We developed an optimization recipe to achieve minimum weighted average reflection structure arhitecture. Depositing 15 nm $SiO_2$ thin film, one of the minimum reflection is obtained for hexagonal array type nanopillar structures. Later, with step coverage of $\mathbf{s/t} = 0.2$, the weighted average reflection is reduced as low as 2% which is one of the lowest reflection reported in the literature for this type of structures and to our knowledge this work is the first to optimize these type of nanostructures in terms of pillar slope, filling ratio, pillar diameter, pillar height, step coverage parameters at the same time in one optimization process.

These modified nanostructured surfaces concept is useful for photonic device applications having thin film silicon or active absorbing semiconducting material for optical energy harvesting through low surface reflection over a broadband optical spectrum [19]. In broad sense, thin film solar cells, photodetectors, phototransistors are the potential applications of these nanostructured surfaces. We used light scattering mechanisms with slope angle of the nanopillars and nonconformal coating of thin film dielectrics and nanopillar photonic crystals arrays light trapping mechanisms in order to achieve low reflection over a broadband spectrum.

For future study, we will work on the absorption of the incident power for solar cell structures. Since the low reflection does not guarantee the optimum quantum efficiency in the solar cells and photodetectors, we have to optimize the absorption in the active layer of the actual photonic device. We will also demonstrate these simulations result in the solar cells and photodetectors in our future research.

**Acknowledgements** This work is funded by TUBİTAK ARDEB 1001 project under project number 219M280. Computing resources were supported by AGÜ (Abdullah Gul University). I would like to thank my colleagues Evren Mutlugün and Mehmet Şahin for valuable discussions on the subject.

**Author Contributions** Material preparation, data collection and analysis and manuscript writing were performed by Turgut TUT.

**Funding** This work was supported by Tubitak 1001 program under the grant number 219M280.

**Data Availability** The datasets used in the plots and they were already presented in the manuscript. However, the raw data used to generate the

figures in the manuscript are available from the corresponding author on reasonable request.

## Declarations

**Competing Interests** The author has no relevant financial or non-financial interests to disclose.

**Ethics Approval** Not applicable for this paper.

**Consent to Participate** Not applicable.

**Consent to Publish** Not applicable.

## References


1. Campbell P, Green MA (1987) Light trapping properties of pyramidally textured surfaces. J Appl Phys 62(1):243–249
2. Boden SA, Bagnall DM (2008) Tunable reflection minima of nanostructured antireflective surfaces. Appl Phys Lett 93(133108). https://doi.org/10.1063/1.2993231
3. Boden SA, Bagnall DM (2010) Optimization of moth-eye antireflection schemes for silicon solar cells. Prog Photovolt 18(3):195–203
4. Chattopadhyay S, Huang YF, Jen YJ, Ganguly A, Chen KH, Chen LC (2010) Anti-reflecting and photonic nanostructures. Mater Sci Eng R-Rep 69(1–3):1–35
5. Hadobas K, Kirsch S, Carl A, Acet M, Wassermann EF (2000) Reflection properties of nanostructure-arrayed silicon surfaces. Nanotechnology 11(3):161–164
6. Huang YF, Chattopadhyay S, Jen YJ, Peng CY, Liu TA, Hsu YK, Pan CL, Lo HC, Hsu CH, Chang YH, Lee CS, Chen KH, Chen LC (2007) Improved broadband and quasi-omnidirectional anti-reflection properties with biomimetic silicon nanostructures. Nat Nanotechnol 2(12):770–774
7. Kanamori Y, Sasaki M, Hane K (1999) Broadband antireflection gratings fabricated upon silicon substrates. Opt Lett 24(20):1422–1424
8. Lalanne P, Morris GM (1997) Antireflection behavior of silicon subwavelength periodic structures for visible light. Nanotechnology 8(2):53–56
9. Pai YH, Lin YC, Tsai JL, Lin GR (2011) Nonlinear dependence between the surface reflectance and the duty-cycle of semiconductor nanorod array. Opt Express 19(3):1680–1690
10. Sai H, Fujii H, Arafune K, Ohshita Y, Kanamori Y, Yugami H, Yamaguchi M (2007) Wide-angle antireflection effect of subwavelength structures for solar cells. Jpn J Appl Phys Part 1-Regular Papers Brief Commun Rev Papers 46(6A):3333–3336
11. Sai H, Fujii H, Arafune K, Ohshita Y, Yamaguchi M, Kanamori Y, Yugami H (2006) Antireflective subwavelength structures on crystalline Si fabricated using directly formed anodic porous alumina masks. Appl Phys Lett 88(201116). https://doi.org/10.1063/1.2205173
12. Sai H, Kanamori Y, Arafune K, Ohshita Y, Yamaguchi M (2007) Light trapping effect of submicron surface textures in crystalline Si solar cells. Prog Photovolt 15(5):415–423
13. Shin JC, Chanda D, Chern W, Yu KJ, Rogers JA, Li XL (2012) Experimental study of design parameters in silicon micropillar array solar cells produced by soft lithography and metal-assisted chemical etching. IEEE J Photovolt 2(2):129–133
14. Seliger P, Mahvash M, Wang CM, Levi AFJ (2006) Optimization of aperiodic dielectric structures. J Appl Phys 100(3)
15. Callahan DM, Munday JN, Atwater HA (2012) Solar cell light trapping beyond the ray optic limit. Nano Lett 12(1):214–218
16. Spinelli P, Verschuuren MA, Polman A (2012) Broadband omnidirectional antireflection coating based on subwavelength surface Mie resonators. Nat Commun 3(692). https://doi.org/10.1038/ncomms1691
17. Wang KXZ, Yu ZF, Liu V, Cui Y, Fan SH (2012) Absorption enhancement in ultrathin crystalline silicon solar cells with antireflection and light-trapping Nanocone gratings. Nano Lett 12(3):1616–1619
18. Boroumand J, Das S, Vazquez-Guardado A, Franklin D, Chanda D (2016) Unified electromagnetic-electronic design of light trapping silicon solar cells. Sci Rep 6(31013). https://doi.org/10.1038/srep31013
19. Shir D, Yoon J, Chanda D, Ryu JH, Rogers JA (2010) Performance of ultrathin silicon solar microcells with nanostructures of relief formed by soft imprint lithography for broad band absorption enhancement. Nano Lett 10(8):3041–3046
20. Yu KJ, Gao L, Park JS, Lee YR, Corcoran CJ, Nuzzo RG, Chanda D, Rogers JA (2013) Light trapping in ultrathin monocrystalline silicon solar cells. Adv Energy Mater 3(11):1401–1406
21. Chong TK, Wilson J, Mokkapati S, Catchpole KR (2012) Optimal wavelength scale diffraction gratings for light trapping in solar cells. J Opt 14(024012). https://doi.org/10.1088/2040-8978/14/2/024012
22. Branham MS, Hsu WC, Yerci S, Loomis J, Boriskina SV, Hoard BR, Han SE, Chen G (2015) 15.7% efficient 10-mu thick crystalline silicon solar cells using periodic nanostructures. Adv Mater 27(13):2182
23. Garnett E, Yang PD (2010) Light trapping in silicon nanowire solar cells. Nano Lett 10(3):1082–1087
24. Karakasoglu I, Wang KXZ, Fan SH (2015) Optical-electronic analysis of the intrinsic behaviors of nanostructured ultrathin crystalline silicon solar cells. ACS Photonics 2(7):883–889
25. Lee SM, Biswas R, Li WG, Kang D, Chan L, Yoon J (2014) Printable nanostructured silicon solar cells for high-performance, large-area flexible photovoltaics. ACS Nano 8(10):10507–10516
26. Mavrokefalos A, Han SE, Yerci S, Branham MS, Chen G (2012) Efficient light trapping in inverted nanopyramid thin crystalline silicon membranes for solar cell applications. Nano Lett 12(6):2792–2796
27. Weinstein LA, Hsu WC, Yerci S, Boriskina SV, Chen G (2015) Enhanced absorption of thin-film photovoltaic cells using an optical cavity. J Opt 17(055901). https://doi.org/10.1088/2040-8978/17/5/055901
28. Zhou DY, Biswas R (2008) Photonic crystal enhanced light-trapping in thin film solar cells. J Appl Phys 103(093102). https://doi.org/10.1063/1.2908212
29. Spinelli P, Polman A (2014) Light trapping in thin crystalline Si solar cells using surface Mie Scatterers. IEEE J Photovolt 4(2):554–559
30. Mutitu JG, Shi SY, Chen CH, Creazzo T, Barnett A, Honsberg C, Prather DW (2008) Thin film silicon solar cell design based on photonic crystal and diffractive grating structures. Opt Express 16(19):15238–15248
31. Bielawny A, Upping J, Miclea PT, Wehrspohn RB, Rockstuhl C, Lederer F, Peters M, Steidl L, Zentel R, Lee SM, Knez M, Lambertz A, Carius R (2008) 3D photonic crystal intermediate reflector for micromorph thin-film tandem solar cell. Phys Status Solidi A-Appl Mater Sci 205(12):2796–2810
32. Palik E (1985) Handbook of optical constants of solids, 1st ed. Academic, Cambridge
33. Park H, Dan Y, Seo K, Yu YJ, Duane PK, Wober M, Crozier KB (2014) Filter-free image sensor pixels comprising

silicon nanowires with selective color absorption. Nano Lett 14(4):1804–1809
34. Tut T, Dan YP, Duane P, Yu Y, Wober M, Crozier KB (2012) Vertical waveguides integrated with silicon photodetectors: Towards high efficiency and low cross-talk image sensors. Appl Phys Lett 100(043504). https://doi.org/10.1063/1.3678019
35. Sopori BL, Pryor RA (1982) Design of antireflection coatings for textured silicon solar cells. Solar Cells 8:249–261
36. Guardado AV, Boroumand J, Franklin D, Chanda D (2018) Broadband angle-independent antireflection coatings on nanostructured light trapping solar cells. Phys Rev Mater 2:035201
37. Yan W, Dottermusch S, Reitz C, Richards BS (2016) Hexagonal arrays of round-head silicon nanopillars for surface anti-reflection applications. Appl Phys Lett 109:143901
38. Li J, Yu H, Wong SM, Zhang G, Sun X, Lo PG, Kwong D (2009) Nanopyramid structure for ultrathin c-Si tandem solar cells. Appl Phys Lett 95:033102
39. Lin C, Huang N, Povinelli ML (2011) Effect of aperiodicity on the broadband reflection of silicon nanorod structures for photovoltaics. Opt Express 20(1):125–132
40. Proust J, Fehrembach A, Bedu F, Ozerov I, Bonod N (2016) Optimized 2D array of thin silicon pillars for efficient antireflective coatings in the visible spectrum. Sci Rep 6:24947
41. Kim J, You S (2021) Surface texturing of Si with periodically arrayed oblique nanopillars to achieve antireflection. Materials 14:380